Tropical Climate Variability: Interactions across the Pacific, Indian, and Atlantic Oceans

Jules B. Kajtar*[1,2], Agus Santoso[1,2], Matthew H. England[1,2], and Wenju Cai[3]

[1] Australian Research Council's Centre of Excellence for Climate System Science, Australia

[2] Climate Change Research Centre, University of New South Wales, NSW, Australia

[3] CSIRO Marine and Atmospheric Research, Aspendale, Victoria, Australia

* Corresponding author: Jules B. Kajtar; j.kajtar@unsw.edu.au; Telephone: +61 (0)2 9385 9766; Facsimile: +61 (0)2 9385 8969

Keywords: ENSO, Indian Ocean Dipole, Indian Ocean Basinwide Mode, Atlantic Niño, Tropical variability, Climate modes

Acknowledgements

This study was supported by the Australian Research Council's Centre of Excellence for Climate System Science. This research was undertaken with the assistance of resources from the National Computational Infrastructure (NCI), which is supported by the Australian Government. We acknowledge the World Climate Research Programme's Working Group on Coupled Modelling, which is responsible for the Coupled Model Intercomparison Project (CMIP), and we thank the climate modelling groups for producing and making available their model output. We also acknowledge the observational reconstructions provided the National Centers for Environmental Prediction (NCEP), the National Center for Atmospheric Research (NCAR), Climate Prediction Center Merged Analysis of Precipitation (CMAP), and the Hadley Centre.

Abstract

Complex interactions manifest between modes of tropical climate variability across the Pacific, Indian, and Atlantic Oceans. For example, the El Niño-Southern Oscillation (ENSO) extends its influence on modes of variability in the tropical Indian and Atlantic Oceans, which in turn feed back onto ENSO. Interactions between pairs of modes can alter their strength, periodicity, seasonality, and ultimately their predictability, yet little is known about the role that a third mode plays. Here we examine the interactions and relative influences between pairs of climate modes using ensembles of 100-year partially coupled experiments in an otherwise fully coupled general circulation model. In these experiments, the air-sea interaction over each tropical ocean basin, as well as pairs of ocean basins, is suppressed in turn. We find that Indian Ocean variability has a net damping effect on ENSO and Atlantic Ocean variability, and conversely they each promote Indian Ocean variability. The connection between the Pacific and the Atlantic is most clearly revealed in the absence of Indian Ocean variability, and our model runs suggest a weak damping influence by Atlantic variability on ENSO, and an enhancing influence by ENSO on Atlantic variability.

1. Introduction

Modes of tropical climate variability, such as the El Niño-Southern Oscillation (ENSO), the Indian Ocean Basinwide Mode (IOBM), the Indian Ocean Dipole (IOD), and the Atlantic Equatorial Mode (sometimes referred to as the Atlantic Zonal Mode, or Atlantic Niño) interact most readily via the atmosphere. Sea surface temperature anomalies (SSTAs) in the tropics drive changes in the Walker Circulation, which in turn influence SSTAs in remote regions, hence forming a teleconnection (e.g., Lau and Nath 1996; Klein et al. 1999; Alexander et al. 2002). Through this atmospheric teleconnection mechanism, modes in one ocean basin can be damped, enhanced, or even entirely generated by a mode in another ocean basin. Oceanic pathways also provide the means for inter-basin interactions, although at lag times typically beyond several months. Whilst the literature is rich on the interactions between ENSO and each of the tropical modes in the Indian and Atlantic Oceans, few studies have examined the possible interactions between the Indian and Atlantic modes, apart from the Atlantic influence on the Indian monsoon (e.g. Kucharski et al. 2008, Losada et al. 2010). Furthermore, if all three tropical basins are strongly coupled, then interactions between any two basins can be influenced or modulated by the third ocean basin. This aspect, which has previously been neglected in the literature, will be considered here. A better understanding of these highly complex inter-basin interactions is relevant for improving climate prediction, especially for ENSO (e.g. Izumo et al. 2010, Keenlyside et al. 2013).

ENSO is a manifestation of complex internal dynamics within the Pacific Ocean, but it is now widely recognised that modes of variability in the Indian and Atlantic oceans also influence the air-sea feedback processes that govern ENSO characteristics (e.g., Dommenget et al. 2006; Izumo et al. 2010; Ding et al. 2012; Santoso et al. 2012; McGregor et al. 2014; Polo et al. 2014; Terray et al. 2015; Kucharski et al. 2016). It is not possible to determine the interaction dynamics from observations and standard climate models alone due to the coupled nature of these modes of variability. Instead, the problem needs to be studied in model experiments whereby individual modes are nullified. This can be achieved by eliminating air-sea interactions over a region of variability, so that the atmosphere does not respond to the SSTAs associated with these remote modes. Such earlier ‘partial coupling’ studies concluded that Indian Ocean variability tends to enhance ENSO (Barsugli and Battisti 1998; Yu at al. 2002; Wu and Kirtman 2004). However, many of these studies were based on a single experiment, with short run-time (approximately 50 years), or using simplified

GCMs. The robustness of this conclusion was put into doubt with higher resolution models and longer experiments (Dommenget et al. 2006; Santoso et al. 2012; Terray et al. 2015). While the IOD may play a role in initiating ENSO events (e.g., Luo et al. 2010; Izumo et al. 2010), Santoso et al. (2012) showed that Indian Ocean variability as a whole exerts a net damping influence on ENSO via the IOBM.

The climatic connections between the Pacific and Indian Oceans are further complicated by the presence of the Indonesian Throughflow (ITF). The ITF typically transports a large volume of water (Potemra 1999; Gordon 2005; Wijffels et al. 2008) and heat (Vranes et al. 2002; England and Huang 2005) from the Pacific to the Indian Ocean, but it exhibits interannual variability which is linked to ENSO and the Indian Ocean modes (Meyers 1996; England and Huang 2005; van Sebille et al. 2014; Sprintall and Revelard 2014). Its significance in the global context is exhibited by model experiments with a blocked ITF, where the mean climate and modes of variability are greatly altered (Song et al. 2010; Santoso et al. 2011). It has been recently suggested that Indian Ocean variability can influence ENSO via Kelvin wave propagation through the ITF (Yuan et al. 2013) at longer time lags. However, a recent study by Izumo et al. (2015) argued that the atmospheric bridge mechanism is more dominant for Indo-Pacific interactions. The robustness of the atmospheric bridge is attested by the fact that the Indo-Pacific feedback interactions persist even in the absence of the ITF (Kajtar et al. 2015).

On interannual time scales, ENSO and variability in the tropical Atlantic basin interact via the atmospheric bridge. The Atlantic Equatorial Mode (AEM), which is the dominant mode of variability in the tropical Atlantic Ocean (Zebiak 1983), displays ENSO-like characteristics (Keenlyside and Latif 2007; Jansen et al. 2009), with SSTAs across the central to eastern equatorial Atlantic Ocean. The relationship between ENSO and the AEM is complex, and predicting the state of the Atlantic Ocean based on the precedence of an ENSO event is not reliable (Saravanan and Chang 2000; Chang et al. 2006; Rodrigues et al. 2011; Lübbecke and McPhaden 2012; Taschetto et al. 2015). In contrast, knowledge of the Atlantic Ocean state can improve ENSO prediction (Frauen and Dommenget 2012; Keenlyside et al. 2013). Frauen and Dommenget (2012) used a GCM, albeit with a simplified ocean model, to demonstrate that the Atlantic Ocean has no net discernible influence on ENSO characteristics, but does influence the state of the Pacific Ocean that is relevant for ENSO prediction. Other studies have shown that an Atlantic Niño (the warm phase of the AEM) tends to favour the development of a La Niña in the Pacific (Ding et al. 2012; Polo et al. 2014). Furthermore, it appears that this relationship has strengthened in recent decades (Rodríguez-Fonseca et al. 2009) and is likely associated with multi-decadal variability (Latif 2001; Martín-Rey et al. 2014; McGregor et al. 2014).

Despite the extensive literature on the Indian and Atlantic Ocean influence on ENSO, few studies (e.g. Dommenget et al. 2006; Frauen and Dommenget 2012; Terray et al. 2015) have examined the role of each within the same modelling framework. These studies agree that Indian Ocean variability damps ENSO, but Terray et al. (2015) point to a weak damping influence by the Atlantic on ENSO, whereas the other studies found none. Terray et al. (2015) also show that decoupling either basin tends to shift ENSO to longer periods. It is also important to note, however, that many coupled models suffer from strong SST biases in the equatorial Atlantic (Ritcher et al. 2014), and hence any comparison between coupled and partially coupled experiments may be compromised by internal model biases.

In this study we will examine, for the first time, the interactions of tropical models of variability between each of the Pacific, Atlantic, and Indian Oceans, all within the same coupled GCM. In particular we expand on very small pool of literature on the Indo-Atlantic coupling (e.g. Kucharski et al. 2008, McGregor et al. 2014), which may play a role in modulating the interactions between ENSO and other modes of variability. We ran sets of five-member, 100-year, partially coupled experiment ensembles in an otherwise fully coupled GCM. In addition to sequentially nullifying the air-sea interactions over each tropical ocean basin individually, we ran further experiments with pairs of ocean basins decoupled. The rationale behind decoupling pairs of ocean basins is to eliminate the influence that a third ocean may play on interactions between modes in the first two, thus helping to infer the role of the third ocean basin. In essence, this study aims to build a global picture of interactions between climate modes across the tropics with potential implications for their predictability. We focus on the dominant modes in the tropics, namely ENSO, the IOD, the IOBM, and the AEM, since they readily interact via induced changes to the Walker Circulation. We focus our analysis on changes to the strength and period of the modes by examining the monthly standard deviations and power spectral densities of the relevant SST indices (Section 3). We then demonstrate the zonal wind stress influences by which the modes interact (Section 4).

2. The climate simulations

2.1 Model description and experimental setup

The simulations were performed with version 1.2 of the Commonwealth Scientific and Industrial Research Organisation (CSIRO) Mk3L general circulation model (GCM; Phipps 2010; Phipps et al. 2013). The atmospheric GCM (AGCM) has a resolution of ~ 5.6º longitude × ~ 3.2º latitude, with 18 levels in the hybrid vertical coordinate. The oceanic GCM (OGCM) has resolution ~ 2.8º longitude × ~ 1.6º latitude, and 21 levels in the vertical z-coordinate. The OGCM was first spun up for 7000 years, and then the ocean surface state was used to spin up the AGCM for 100 years. To maintain a more realistic climatology and minimise drifts, the AGCM and OGCM were then coupled with constant, but seasonally varying, flux adjustment terms applied to the surface heat flux, surface salinity tendency, and surface momentum fluxes. The terms are derived at the end of the spin-up phase, and not restored towards observations during the coupled run.

Following the initial spin-up, the coupled model was integrated for 1550 years, with CO_2 fixed at the preindustrial level of 280 ppm, since here we are focussing on the dynamics without anthropogenic forcing. The last 300 years of this run is referred to as the control simulation (CTRL). This 300-year run was split into five 100-year ensemble members, with 50-year intervals for the starting year of each set, i.e. the first set starts at year 1, the second at year 51, and so on, until year 201 for the fifth set. The 100-year partial coupling experiments were then initialized with the climate state at each of these epochs. In these runs, the air-sea interaction over a single or pair of ocean basins was suppressed by fixing SST to the climatological seasonal mean field from the first 200 years of the model control run (as per the methodology of Baquero-Bernal et al. 2002; Behera et al. 2005; Dommenget et al. 2006; Santoso et al. 2012; Kajtar et al. 2015). In this way, the atmosphere responds only to the seasonally varying climatological SST over the decoupled region, and hence any modes of variability in that region are nullified.

We note that one may also choose to nudge SST toward observed climatology. However, as shown by Terray et al. (2015), the decoupling effect on tropical climate variability in a given ocean basin will also contain changes resulting from an altered mean state within that basin. In the case of Terray et al. (2015), nudging the Indian or Atlantic toward their respective observed SST climatology results in a more realistic Pacific climatology. At the same time, the ENSO response becomes stronger, but still exhibits similar tendencies as in the case of nudging toward model climatology. To isolate the effects of only the remote forcing, we chose to perform the decoupling by nudging toward model SST climatology. The flux adjustments in our model assist with maintaining a more realistic climatology, and are applied globally and consistently throughout all experiments, thus ensuring that any of the diagnosed changes are not due to flux adjustments, but to the decoupling of remote SSTAs.

The decoupled regions in our experiments are bounded by 30ºS and 30ºN, and by the coast to the east and west in each ocean basin. As discussed by Santoso et al. (2012), choosing a particular boundary between the Pacific and Indian Oceans may affect the conclusions reached. Nevertheless, in this study we follow their approach in which the western side of the Maritime Continent is considered part of the eastern Indian Ocean, and the eastern side as part of the western Pacific Ocean. The decoupled Pacific, Indian, and Atlantic Ocean experiments are denoted $DCPL_{PO}$, $DCPL_{IO}$, and $DCPL_{AO}$ respectively. The experiments where pairs of ocean basins were decoupled follow a similar nomenclature, i.e. $DCPL_{PO+AO}$, $DCPL_{PO+IO}$, and $DCPL_{AO+IO}$. Note that throughout the text, "decoupling" will refer to the suppression of SST variability over a particular ocean basin. We ran 100-year experiments so that the significance of the interactions between low-frequency modes could be statistically assessed. The mean climate drift over this period in the Mk3L model is negligible.

2.2 Model validation

Mk3L performs relatively well in capturing the mean climatology and tropical modes of variability, albeit with some notable biases. As with many GCMs, Mk3L suffers from the "cold tongue" bias, with overly strong trade winds and lower than observed rainfall, associated with anomalously cold SST extending westward from the eastern equatorial region of each ocean basin (Fig. 1). The dry bias appears to be exacerbated over the Maritime Continent by a shallower than observed thermocline depth in the eastern Indian Ocean which causes overly cold SST in that region (Santoso et al. 2012). Somewhat expected given the overly strong easterly winds in the Pacific, the mean Indonesian Throughflow rate in the model (approximately 21 Sv with a standard deviation of 1.3 Sv; see also Santoso et al. 2011) is substantially larger than the observed estimate of 15 Sv (Sprintall et al. 2014). This is also partly attributed to the coarse model resolution, likely through the joint effect of baroclinicity and relief (JEBAR; England et al. 1992; Santoso et al. 2011).

In order to evaluate the Mk3L model performance in simulating the relevant modes of tropical climate variability, we compare against observations (HadISST) and a set of the historical experiments, over the period 1900-1999, from the Coupled Model Intercomparison Project, phase 5 models (CMIP5; bcc-csm1-1, CanESM2, CCSM4, CNRM-CM5, FGOALS-g2, FGOALS-s2, GFDL-CM3, GFDL-ESM2G, GFDL-ESM2M, HadCM3, HadGEM2-CC, HadGEM2-ES, IPSL-CM5A-LR, IPSL-CM5A-MR, IPSL-CM5B-LR, MIROC4h, MIROC5, MIROC-ESM-CHEM, MPI-ESM-LR, MPI-ESM-MR, MPI-ESM-P, MRI-CGCM3, NorESM1-M, and NorESM1-ME). The modes and their associated characteristic SST indices are given in Table 1. The Mk3L ENSO SST variability has weaker magnitude and peaks 2-3 months earlier than the observed, although it falls well within the overall CMIP5 model range (Fig. 2a). Its period in Mk3L is also slightly longer, with the strongest signal in the 5-7 year band (Fig. 2b). The Atlantic Equatorial Mode (AEM) is also weaker than observed, but has a similar seasonal cycle to the observed, with peak variability around May to August (Fig. 2c). This seasonal cycle is not captured by the CMIP5 multi-model mean, and may be attributed to either strong model biases in the tropical Atlantic (Ritcher et al. 2014) or large model diversity, or both. The observed Atl-3 index shows variability at a range of time-scales with an increasing tendency toward interdecadal timescales; a tendency also seen in the CMIP5 ensemble and Mk3L. Spectral peaks common to those of ENSO are seen in the observed and Mk3L, although in Mk3L the signal is clearly occurring in the 5-7 year band (Fig. 2d). Higher-frequency variability is muted in Mk3L, and is captured by only a few of the CMIP5 models.

Over the Indian Ocean, the IOD in Mk3L is stronger than observed, as with many GCMs (Fig. 2e), which is associated with the shallower than observed thermocline in the eastern Indian Ocean (Cai and Cowan 2013). Also associated with a shallower thermocline are overly persistent cool SSTAs in a limited region of the eastern Indian Ocean during a positive IOD, thus slightly affecting the representation of the warm phase of the IOBM, and vice versa for the negative IOD (see Fig. 2 of Santoso et al. 2012). Nevertheless, the variability and seasonality of the model IOBM agrees well with observations (Fig. 2g). Like observations, the IOD and IOBM in Mk3L exhibit variability that coincides with ENSO time-scales, but again in Mk3L this is in the 5-7 year band (Figs. 2f,h). This correspondence is not clear in the CMIP5 ensemble due to the large model diversity. The common periodicity signal across the indices, apparent in the observations and Mk3L, indicates a coupling across the modes. These interactions will be disentangled and studied using our partial coupling experiments.

We now focus further on evaluating the model's performance in simulating the tropical Atlantic climate, since the performance in the Indo-Pacific region has been previously documented in detail (Santoso et al. 2011; 2012). Firstly, note that the SST bias across the tropical Atlantic is slightly different to most other coupled models. The CMIP3 and CMIP5 models tend to show a temperature gradient across the basin that is warmer in the east, opposite to what is observed (see Fig. 1 of Richter et al. 2014). Yet the Mk3L model correctly captures the sign of this gradient (apparent in Fig. 1a, b). The spatial pattern of the model's first empirical orthogonal function (EOF) of June to August SST (Fig. 3a), i.e., the AEM peak season, shows some agreement with the observed (Fig. 3b). The southeastern branch is absent in the model, but it largely captures the zonal mode structure along the equator. Many CMIP5 models either do not exhibit the AEM as the first EOF, or at all (Richter et al. 2014). The first EOF explains a similar percentage of the total variance in the model (32%; 24% for EOF-2) and in the observed (47%; 25% for EOF-2). The correlation between the Atl-3 index and the SST field, both averaged over June to August, reveals a good agreement overall in the variability pattern between the model and observed (Fig. 3c,d), except for a negative correlation at ~10ºN that is not seen in the reanalysis fields. Despite the shortcomings of the Mk3L model, it broadly captures the tropical climate modes, at least within the expected range of state-of-the-art CMIP5 model performance. Finally, we note that its coarse resolution makes it suitable for running large ensembles of century-scale experiments, such as those undertaken here.

3. Changes in amplitude and periodicity of the modes

We begin by examining the changes to the amplitude, and then later the periodicity, of the dominant tropical modes in the partial coupling experiments. The modes are each characterised by area-averaged SST indices that display distinct seasonality (outlined in Table 1), and so we examine changes to the monthly standard deviation of the SST indices.

Suppressing tropical Indian Ocean SST variability in the $DCPL_{IO}$ experiments increases the monthly standard deviation of the Niño-3.4 index relative to CTRL (Fig. 4a), indicating stronger ENSO in $DCPL_{IO}$. The increase is statistically significant throughout most of the calendar year (October to July), as indicated by the separation between the confidence intervals associated with the CTRL and $DCPL_{IO}$ experiments. This change indicates that the presence of SST variability over the tropical Indian Ocean acts to damp ENSO variability, in agreement with earlier studies (Dommenget et al. 2006; Terray et al. 2015), and with Santoso et al. (2012) who used a larger ensemble in the same MK3L model. The mechanisms by which the Indian Ocean climate modes influence ENSO evolution are described in detail in Section 4.

The influence of the Atlantic Ocean on ENSO is less clear. The confidence interval of Niño-3.4 in the $DCPL_{AO}$ experiments overlaps that of CTRL in each calendar month (Fig. 4a). Closer inspection of the individual ensemble members reveals that the variability is weaker relative to CTRL in two members, but stronger in the remaining three (figure not shown). This is in contrast to $DCPL_{IO}$, which exhibits stronger ENSO variability across all ensemble members. The inconsistent changes underscore the importance of ensemble experiments. Terray et al. (2015) found a weak enhancement of ENSO variability, although they perform twin partial coupling experiments, nudged towards either observed or model climatological SST (an issue not assessed here). Dommenget et al. (2006) found no clear overall change in ENSO variance when the Atlantic is decoupled in their single 500-year experiment, but they did not examine the change in shorter sub-periods. Nevertheless, it is important to keep in mind that this inconsistent response does not mean that the Atlantic Ocean exerts no influence on ENSO. Frauen and Dommenget (2012), for instance, concluded that the Atlantic Ocean plays a role in the predictability of ENSO, despite having no clear impact on its dynamics. The inconsistency can also arise due to multi-decadal variability in Atlantic-Pacific connection (Latif 2001; Rodríguez-Fonseca et al. 2009; Martín-Rey et al. 2014; McGregor et al. 2014).

Care should be taken when inferring the actual impact of the Atlantic Ocean on ENSO based on decoupling the Atlantic alone, without considering changes that could occur in the Indian Ocean resulting from a decoupled Atlantic. The same can be said about decoupling the Indian Ocean to diagnose its isolated effect on ENSO when Atlantic variability is still present in $DCPL_{IO}$. Further insights into this interplay can be garnered when both the Atlantic and Indian Oceans are decoupled ($DCPL_{AO+IO}$). As shown in Fig. 4a, decoupling both the Indian and Atlantic Oceans enhances the variability of ENSO more strongly than decoupling the Atlantic or Indian Ocean alone, which is consistent with Dommenget et al. (2006) and Frauen and Dommenget (2012). Interestingly, the enhanced variability seen in $DCPL_{AO+IO}$ relative to $DCPL_{IO}$ is strongest during May to August, coinciding with the peak season of AEM variability. This could imply that Atlantic variability exerts a more consistent effect on ENSO growth than what is inferred from $DCPL_{AO}$ in which Indian Ocean variability is present. It is also possible that the impact of the Indian Ocean on ENSO is in actuality greater without the presence of Atlantic variability. In other words, in $DPCL_{IO}$, the Atlantic variability may be altered upon decoupling the Indian Ocean in such a way that it limits the enhancement of ENSO amplitude due to the removal of Indian Ocean variability. Concurrent removal of Atlantic variability then leads to more amplified ENSO in $DCPL_{AO+IO}$ compared to $DCPL_{IO}$. This would imply that the Atlantic variability has a net damping effect on ENSO in our model – different to what is inferred from the $DCPL_{AO}$ runs alone. A damping influence on ENSO by the Atlantic, but smaller than the damping influence by Indian Ocean variability, is consistent with Terray et al. (2015) based on their individual basin decoupling experiments. In any case, our $DCPL_{AO+IO}$ result compared with $DCPL_{IO}$ and $DCPL_{AO}$ suggests that there are potential interactions occurring between the Atlantic and Indian Ocean variability. This will become clearer below.

As shown in Fig. 4b, the change in AEM variability is significantly different from CTRL due to removal of the Indian Ocean alone ($DCPL_{IO}$), implying a potential damping role of Indian Ocean variability on AEM in CTRL. However, it is also possible that the AEM enhancement is due to the enhanced ENSO arising from a decoupled Indian Ocean (Fig. 4a). We argue that it is both, but the Indian Ocean damping is more dominant, for the following reasons. Decoupling the Pacific Ocean ($DCPL_{PO}$) does not result in net significant changes to the AEM, except weakened Atl-3 index outside the boreal summer peak of the AEM (Fig. 4b). If the enhancing effect of ENSO were dominant, then we would expect the weakening of the AEM to be significant. The fact that it is not can be explained by a reduced damping effect of the Indian Ocean (in $DCPL_{PO}$), since Indian Ocean variability is weakened when the Pacific is decoupled (Fig. 4c,d). Removing Indian Ocean variability while the Pacific remains decoupled ($DCPL_{PO+IO}$; i.e., no ENSO enhancing effect and no Indian Ocean damping) exhibits a slight increase in AEM amplitude, but the change is not statistically significant from either CTRL or $DCPL_{IO}$ during the peak season. This confirms that the significant AEM enhancement seen in $DCPL_{IO}$ is due to primarily an absence of Indian Ocean variability and to a lesser extent the presence of a stronger ENSO. Thus, the Indian Ocean variability in our model has a net damping effect on AEM, while the ENSO tends to enhance AEM.

Decoupling the Pacific Ocean reduces the amplitude of the Indian Ocean Dipole, consistent with previous studies (Fischer et al. 2005; Behera et al. 2006). The reduction of DMI standard deviation in $DCPL_{PO}$ relative to CTRL is statistically significant for all months, but weakest during boreal autumn when IOD peaks (Fig. 4c). Decoupling both the Atlantic and the Pacific ($DCPL_{PO+AO}$) shows similar effect as $DCPL_{PO}$, indicating that the Atlantic has little influence on IOD amplitude. This is confirmed by $DCPL_{AO}$, which shows a weak change to the DMI standard deviation. Thus, in our model the Pacific Ocean partly drives IOD variability, but there is still substantial Pacific-independent component. This supports the notion that while ENSO can generate IOD, the IOD itself is intrinsically a mode internal to the Indian Ocean.

The enhancing influence of Pacific Ocean variability on the IOBM is more pronounced than its influence on the IOD, since the variability of the BWI is reduced during most months, but most importantly throughout its peak season when the Pacific is decoupled ($DCPL_{PO}$ and $DCPL_{PO+AO}$). There is also a noticeable change in the seasonality of the BWI, which can be seen by comparing $DCPL_{PO}$ and $DCPL_{PO+AO}$ relative to CTRL (Fig. 4d). While this at a first glance supports the suggestion that the IOBM is largely a response to ENSO (Klein et al. 1999; Lau and Nath 2003; Du et al. 2009), the fact that decoupling the Pacific does not entirely remove the IOBM also suggests that the IOBM can occur without ENSO. There is also an indication of an Atlantic influence. Decoupling the Atlantic while the Pacific remains decoupled further reduces the IOBM amplitude, although the associated changes occur outside the peak season of the IOBM. This is supported by $DCPL_{AO}$ result showing reduced variability in those months, thus revealing that Atlantic variability enhances the IOBM in CTRL.

The weak change in seasonality of all modes under each partial coupling experiment (Fig. 4), suggests they are, to a varying extent, internally generated modes in their respective basins. This demonstrates a certain degree of independence between the modes. However, the weak change in seasonality may also be a result of replacing the SSTAs with the model SST climatology. It is important to note that the response may be different if using observed SST climatology for the partial coupling. For example, Terray et al. (2015) find that the seasonality of ENSO is more pronounced when nudged toward the observed SST climatology.

The changes described above involve shifts in the periodicity of each mode. This is clearly shown in the power spectral densities (PSDs; Fig. 5). The most striking feature is the dominant variability in the 5-7 year band in each index in the control experiments, which is also the dominant ENSO frequency in Mk3L. This common periodicity across the three basins suggests the timescale at which the inter-basin coupling occurs. The partial coupling experiments reveal the collapse of variability over this 5-7 year frequency band, resulting in variability tending to be skewed towards longer periodicity. The shift in ENSO variability toward longer periods in the partial coupling experiments relative to CTRL (Fig. 5a) is in agreement with previous studies (e.g., Dommenget et al. 2006; Santoso et al. 2012; Terray et al. 2015). Decoupling the Indian Ocean alone enhances variability in the 7-9 year band, thus accounting for the stronger ENSO amplitude as seen in the monthly standard deviation of the Niño-3.4 index (Fig. 5a). The Niño-3.4 PSD reddens in $DCPL_{AO}$ without exhibiting any characteristic frequency, while $DCPL_{AO+IO}$ exhibits a peak in the 9-15 year band. These results suggest that the ENSO evolution in Mk3L could be more sluggish without Indian and Atlantic variability. Both the Indian and Atlantic Ocean variability appear to play a role in setting that 5-7 year ENSO periodicity. Shift toward longer periodicity is also seen in the AEM in the absence of Indian and Pacific variability (Fig. 5b), while it is not as apparent for the IOD and IOBM, which involve primarily a collapse in variability, particularly at the 5-7 year timescales (Fig. 5c,d).

Our findings can be summarised as follows:

- There are interactions between modes of variability across the three tropical oceans.
- Indian and Atlantic variability has a net damping effect on ENSO magnitude and increases the rapidity of ENSO evolution.
- Indian Ocean variability has a net damping effect on the AEM, while ENSO tends to enhance the AEM.
- IOD variability is enhanced by ENSO, but there is little influence by Atlantic variability.
- IOBM variability is enhanced by ENSO and to a weaker extent by Atlantic variability.
- Decoupling any ocean basin collapses variability in the 5-7 year primary ENSO frequency band and tends to shift modes toward longer periodicity.

4. Interbasin feedback interactions via atmospheric bridge

As has been shown in many previous studies (e.g., Lau and Nath 1996; Klein et al. 1999; Alexander et al. 2002; Dayan et al. 2015; Kajtar et al. 2015), interactions between modes of variability across different basins readily occur via the atmospheric bridge. SSTAs across the equatorial seas associated with these modes of variability drive anomalies in the Walker Circulation. These atmospheric disturbances generate wind stress anomalies over remote seas, which impinge on the oceanic dynamics by, for example, forcing Kelvin waves. In this section we examine the composite evolution of the SST anomalies (Fig. 6) and the equatorial zonal wind stress anomalies (Fig. 7, 8) in each experiment to show how the changes in each of the modes of variability under partial coupling can be explained via alterations to the Walker Circulation that connects the climate in the three tropical basins. The composites in Fig. 6-8 are produced by first constructing annual time-series of each SST index, averaged over the corresponding peak seasons in each ensemble and experiment (Table 1), and then selecting the years that exceed one standard deviation of that time-series. For example, El Niño or La Niña events are defined as when the September-December (SOND) average of Niño-3.4 is greater or less than one standard deviation. In cases where the threshold is exceeded in two or more consecutive years, only the year with strongest anomaly is included in the composite, to avoid the inclusion of double events. Note that this compositing approach is valid since there are no significant changes to the seasonality of the modes under the different partial coupling experiments (Fig. 4).

Analysis of the correlations between pairs of modes in the control simulation is also necessary to provide information on the typical interactions, helping to interpret the decoupling experiment results. For example, if the warm phase of the IOBM acts to damp El Niño, but the cool phase is equally likely to co-occur with El Niño (thus rendering a weak correlation between IOBM and ENSO), then the net influence of the decoupled Indian Ocean on ENSO would be expected to be minimal. Hence in the following analysis we show the correlation coefficients between a range of the characteristic SST indices, alongside the observed and CMIP5 values for comparison (Fig. 9). As noted below, some aspects of the CMIP5 results in Fig. 9 clearly illustrate the need for partial coupling experiments in diagnosing inter-basin interactions, which is not otherwise possible from the multi-model statistics.

4.1 El Niño-Southern Oscillation

The Niño-3.4 composite evolution for El Niño and La Niña (Fig. 6a,b; solid lines) reinforces the changes seen in the monthly standard deviation (Fig. 4a). Focussing firstly on the peak season of variability (i.e. Sep(0)-Dec(0), yellow shaded region in Fig. 6a,b), the SSTAs are enhanced in both phases in $DCPL_{IO}$ and $DCPL_{AO+IO}$ relative to CTRL (Fig. 6a,b; red and orange solid lines compared to black), but not in $DCPL_{AO}$ (green solid line compared to black). After the peak ENSO season, the enhancement of $DCPL_{IO}$ relative to CTRL (Fig. 6a,b) reflects the strongest shift in the monthly standard deviation, occurring during the boreal winter and spring (Fig. 4a). Other changes are seen outside of the peak season in all partial coupling experiments, most notably in $DCPL_{AO+IO}$, but these are consistent with lengthening of the periodicity (Fig. 5a).

The enhanced SSTAs are consistent with the absence of the IOBM damping effect (Santoso et al. 2012). The notably stronger Niño-3.4 anomalies in the months following the ENSO peak season (Fig. 6a,b; red solid line compared to black) coincide with IOBM peak occurrence (in a non-decoupled Indian Ocean). It is known that the IOBM induces zonal wind stress (τ^x) anomalies over the western Pacific that oppose the westerly or easterly anomalies associated with eastern Pacific El Niño warming or La Niña cooling (e.g., Kug and Kang 2006; Santoso et al. 2012). The τ^x signature of IOBM is apparent in the CTRL composites between 100°E-160°E during Jan(1) to May(1) (Fig. 7a,e). In response to these western Pacific wind anomalies, oceanic Kelvin waves also act to promote ENSO phase turnabout (Wang et al. 1999a). Consistently, in the absence of these negative feedback processes in $DCPL_{IO}$ and $DCPL_{AO+IO}$, ENSO variability is enhanced and prolonged in those runs (see Section 3). Note that the western Pacific wind anomalies are not solely a remote response to IOBM but are also part of ENSO evolution that is internal to the equatorial Pacific (Watanabe and Jin 2002; Wang et al. 1999b). Thus, even when the IOBM is completely absent in $DCPL_{IO}$ and $DCPL_{AO+IO}$, these western Pacific wind anomalies associated with ENSO still prevail. These western Pacific τ^x anomalies are significantly weaker in the decoupled experiments than in CTRL, and this is particularly so in $DCPL_{IO}$ and $DCPL_{AO+IO}$ in which the IOBM is completely absent (Figs. 7b-d,f-h). The weakened τ^x occurs despite ENSO anomalies being enhanced in those decoupled experiments (Fig. 4a), thus underscoring the impact of the missing IOBM in $DCPL_{IO}$ and $DCPL_{AO+IO}$.

The effect of the IOBM on western Pacific τ^x cannot be clearly inferred in BWI composites from $DCPL_{PO}$ or $DCPL_{PO+AO}$ (Fig. 8j,l,n,p) since its associated SSTAs, although present, become substantially weaker in the absence of ENSO (Fig. 6g,h). Nevertheless, the expected easterly τ^x anomalies are still visible near the Indo-Pacific boundary for positive IOBM (Fig. 8l), and westerly τ^x for negative IOBM (Fig. 8p), confirming the presence of a weak IOBM without ENSO.

The IOBM damping on ENSO is an intrinsic feature of the Indo-Pacific feedback interactions. This stems from the co-occurrence of El Niño with warm IOBM and La Niña with cool IOBM, which is underscored by the strong positive correlation between Niño-3.4 and BWI as seen in the observations, CMIP5 models and Mk3L (Fig. 9g,h). In this way the IOBM wind anomalies tend to consistently damp ENSO. The CMIP5 model spread reveals that there is a tendency for stronger positive correlation between ENSO and IOBM with stronger ENSO and IOBM amplitude. Such tendency makes it challenging to diagnose the effect of IOBM on ENSO using statistical analysis alone, hence reinforcing the need for partially coupled model experiments.

The more severe weakening of western Pacific τ^x anomalies in $DCPL_{AO+IO}$ than in $DCPL_{IO}$ and the lesser weakening in $DCPL_{AO}$ relative to CTRL indicates the potential role of Atlantic variability in enhancing the western Pacific τ^x anomalies that have a damping effect on ENSO in CTRL. This result is consistent with the amplification of Niño-3.4 variability in $DCPL_{AO+IO}$ outside the ENSO peak season (Fig. 4a; Fig. 6a,b). Albeit weak, the τ^x response to Atlantic Niño is visible in the composite plot of Atl-3 with the Indian Ocean decoupled (Fig. 7j,l), with westerly anomalies in the equatorial Atlantic and easterly anomalies in the western Indian Ocean which appear to correspond with further anomalies in the western Pacific towards the end of the calendar year (at Dec(0) between 120ºE and 160ºE). These anomalies are of the opposite sign for Atlantic Niña (Fig. 7n,p). The western Pacific anomalies vary in strength, timing, and position across the ensemble members (figure not shown), and hence appear weak in the ensemble mean. These τ^x signals are not clear with air-sea interactions occurring in the Indian Ocean (Fig. 7k, o), presumably due to interference with Indian Ocean internal variability. With the Atlantic decoupled, such wind anomalies are absent, thus tending to enhance ENSO growth, as seen in $DCPL_{AO+IO}$.

Another way in which Atlantic variability might influence ENSO is via an alteration to Indian Ocean variability. As seen earlier, the Atlantic appears to enhance the IOBM (Fig. 4d), and the IOBM has correspondingly been shown to damp ENSO. Therefore, if the IOBM becomes weaker in the absence of Atlantic variability ($DCPL_{AO}$), the ENSO variability is expected to increase, although it should not be stronger than when the IOBM is completely removed in $DCPL_{AO+IO}$. The composites of Atl-3 indeed show that in correspondence with Atlantic Niño, there is a warm IOBM response (Fig. 6c), and conversely for Atlantic Niña (Fig. 6d). This Atlantic influence on ENSO via the IOBM may explain the enhanced Niño-3.4 anomalies in $DCPL_{AO}$ after Jul(1) (Fig. 6a,b). Such Indian Ocean warming or cooling response can be achieved through Atlantic forced wind stress anomalies in the western tropical Indian Ocean (Fig. 7j,l,n,p) over which ocean advection and entrainment are the dominant factors that generate interannual surface temperature anomalies (Santoso et al. 2010). These easterly/westerly anomalies force a downwelling/upwelling signal in the western Indian Ocean that then propagates eastward as a Kelvin wave (figure not shown), thus promoting the occurrence of a basin-wide warming/cooling pattern. Decoupling the Atlantic alone does not remove the IOBM signal entirely as the IOBM warming/cooling is part of ENSO evolution (Fig. 6a,b, green line with dots), and so any enhancement of ENSO amplitude in $DCPL_{AO}$ is expectedly weaker than when the Indian Ocean is also decoupled (i.e., $DPCL_{AO+IO}$; Fig. 4a, 6a,b). ENSO enhancement in $DCPL_{IO}$ compared to $DCPL_{AO+IO}$ is also limited because decoupling the Indian Ocean tends to enhance the AEM (Fig. 4b), which in turn has a damping effect on ENSO via its tendency to enhance western Pacific τ^x anomalies.

The AEM effects on ENSO described above would be maximal when an El Niño condition co-occurs with a warm AEM, and likewise for co-occurring cool events. However, such a combination has a weak tendency of occurring in our model, and similarly across the CMIP5 models (Fig. 9a-d), unlike the robust ENSO-IOBM relationship (Fig. 9g,h). When we examine the correlation between the two indices with Atl-3 leading by 12 months (figure not shown), we find that the two ensemble members showing a statistically significant negative correlation exhibit a damped ENSO when the Atlantic is decoupled. For the remaining three members, where the correlation is weak or positive, the ENSO is enhanced when the Atlantic is decoupled. These inconsistent connections seem to be in line with recent studies that claim there is varying Atlantic-Pacific connection in observations due to decadal variability (Rodríguez-Fonseca et al. 2009; Martín-Rey et al. 2014; Sasaki et al. 2014; McGregor et al. 2014).

Another factor that can contribute to the lack of consistency is asymmetry between the warm and cool phases of the modes. The SSTA and wind stress composites for Atl-3 (Fig. 6c,d; 7i,m) show that there is an asymmetry in CTRL, namely that Atlantic Niño tends to precede La Niña, but Atlantic Niña tends to follow a La Niña. Indian Ocean variability seems to be the source of this asymmetry, since both phases of the AEM tends to follow ENSO (warm/cool AEM follows El Niño/La Niña) when the Indian Ocean is decoupled. The correlation of Atl-3 averaged over June to August leading December to February Niño-3.4 is close to zero (Fig. 9c,d). This however appears to disagree with observations, which shows a statistically significant negative correlation. The CMIP5 models slightly favour a negative correlation, but many models also display a positive correlation (Kucharski et al. 2015), and the correlation does not appear to be related to the strength in variability of either index across the models.

The IOD generates only weak τ^x anomalies over the Pacific Ocean in $DCPL_{PO+AO}$ (Fig. 8d,h). Santoso et al. (2012) noted that in this way the IOD is conducive for ENSO growth given the dominant IOBM damping effect. The significant positive correlation between Niño-3.4 and DMI at near zero lag is consistent with observations (Annamalai et al. 2005; Santoso et al. 2012), and the CMIP5 models (Fig. 9e,f). The inter-model relationships also show the tendency for stronger ENSO and IOD amplitude to reinforce this positive correlation. Again, analysis of partial coupling experiments suggests that care should be taken when inferring IOD impact on ENSO and vice versa.

4.2 Atlantic Equatorial Mode

The model SST composites reveal that weak Atlantic Niño conditions coincide with the El Niño, and are followed by warm IOBM (Fig. 6a). Similarly, a weak Atlantic Niña coincides with La Niña, followed by cool IOBM (Fig. 6b). The Atlantic Niño is accompanied by westerly τ^x anomalies over the central Atlantic Ocean during April to July (Fig. 7i), and easterly τ^x anomalies with the Atlantic Niña (Fig. 7m). Wind stress anomalies opposing the Atlantic Niño are revealed in composites of El Niño, strongest at one-year lag (Fig. 7a), and also in composites of positive IOBM in CTRL (Fig. 8i). The same holds for Atlantic Niña, and composites of La Niña (Fig. 7e) and negative IOBM (Fig. 8m).

The influence of the IOBM is evidenced by the more significant weakening of the τ^x signal over the Atlantic Ocean in $DCPL_{IO}$ (Fig. 7b,f) compared to any of the other experiments (Fig. 7c,d,g,h). Although weak, these τ^x anomalies are still present even when the Indian Ocean is decoupled ($DCPL_{IO}$), but are more prominent when the Atlantic is also decoupled ($DCPL_{AO+IO}$) – which is expected given the now absent anomalies associated with the AEM. Note that these τ^x anomalies occur during the growth phase, as well as the decay phase of ENSO in the model. As argued by Latif and Grötzner (2000), easterly wind anomalies over equatorial Atlantic during El Niño force downwelling that lead to the formation of an Atlantic Niño six months later. Similarly, westerly wind anomalies during La Niña promote an Atlantic Niña. Thus, here we are looking at both ENSO and IOBM processes that enhance and damp the AEM. Given the results in Section 3 (Fig. 4b), the IOBM damping is the more dominant factor. Interestingly, this Indian Ocean damping effect appears to be supported by the CMIP5 inter-model correlations: there is a negative correlation between the BWI leading Atl-3 correlation and the Atl-3 standard deviation (Fig. 9o). This shows the tendency for models that simulate more occurrences of warm IOBM with Atlantic Niño to have weaker AEM amplitude. This tendency is also supported by the relationship between the ENSO leading AEM correlation with the Atl-3 standard deviation (Fig. 9b), given that El Niño induces warm IOBM. Furthermore, since the IOBM is to a large extent a response to ENSO, it can also be inferred that ENSO damps the AEM indirectly via the IOBM. The effect of ENSO in enhancing the AEM may also be conveyed via the IOD. A positive IOD is associated with easterly τ^x anomalies in the equatorial Atlantic during boreal winter (Fig. 8d), and the opposite for negative IOD (Fig. 8h). However, this is outside the peak season of the AEM, so the effect is expected to be weaker.

4.3 Indian Ocean Modes

The positive IOD is associated with easterly τ^x anomalies across the Indian Ocean basin (Fig. 8a), and the negative IOD with westerly τ^x anomalies (Fig. 8e). Some of these τ^x anomalies can be induced by ENSO, as is clear in the decoupled Indian Ocean runs (Fig. 7b,d). In $DCPL_{AO+IO}$ (Fig. 7d,h), the τ^x anomalies of the opposite sign near the Indo-Pacific boundary are stronger than in $DCPL_{IO}$ (Fig. 7b,f). Nevertheless, ENSO drives τ^x anomalies over the western side of the Indian Ocean that promote the IOD (Annamalai et al. 2003; Fischer et al. 2005). The ENSO-IOD relationship is highlighted by a positive correlation in observations and across models (Fig. 9e,f). The CMIP5 inter-model correlations also suggest a tendency for stronger ENSO-IOD correlation with stronger ENSO or stronger IOD. The AEM also drives τ^x anomalies that are favourable for the IOD (Fig. 7l,p), but the inter-model correlation is weak for Atl-3 leading DMI (Fig. 9i,j). Given the Atl-3 and Niño-3.4 correlation is also not strong, the AEM appears to be secondary in the influence on the IOD compared to ENSO.

As mentioned above, the western Indian Ocean τ^x anomalies associated with the IOD, which are enhanced by ENSO and the AEM, can facilitate the formation of IOBM. Such dynamical association is highlighted by the strong positive correlation between the BWI and DMI (Fig. 9q,r), implying that with enhanced IOD events, stronger IOBM will ensue.

5. Summary

This study investigated the interactions between the dominant modes of climate variability across the tropics, namely ENSO, the AEM, the IOD and the IOBM. Using a series of coupled and partially coupled GCM experiments we inferred the impact between modes on their strength, period, and seasonality. In agreement with earlier studies, we found that Indian Ocean variability acts to damp ENSO via the IOBM (Santoso et al. 2012). Conversely the Pacific enhances both the IOD and IOBM (e.g., Behera et al. 2006). We have highlighted other findings that have not previously been explored in great depth, for instance, the connection between tropical Indian Ocean and Atlantic variability. We found that Atlantic Ocean variability has little influence on the IOD, but enhances the IOBM amplitude. Conversely, Indian Ocean variability has a net damping effect on the AEM. As suggested by the wide range of conflicting literature, the connection between the Pacific and Atlantic Niños and Niñas is complex. Our study has shown that the coupling to the tropical Indian Ocean is a factor that needs to be considered in inferring the Pacific-Atlantic interactive feedbacks. After accounting for the effect of the Indian Ocean, our model experiments reveal that the AEM has a net damping effect on ENSO magnitude in our model, whilst ENSO tends to enhance the AEM.

The dominant ENSO period in the Mk3L model is in the 5-7 year band. We found that decoupling either or both of the Indian and Atlantic Ocean basins shifts the ENSO to longer periods, implying that variability in each plays a role in the faster switching between ENSO phases. The 5-7 year signal is also dominant in the power spectral densities of the other SST indices. The signal vanishes or is reddened in the absence of ENSO variability, thus demonstrating the coupling between ENSO and each of the tropical modes. Nevertheless, our results also show that each mode persists when variability in other basins, in turn and in combination, is removed. Furthermore, apart from slight changes to the IOBM, the overall seasonality of these modes is unchanged. This suggests that ENSO, the IOD, the AEM, and to a lesser extent the IOBM, are largely internally generated modes, despite the fact that the coupling between them influences their overall behaviour.

Although the Atlantic Ocean appears to have a weak damping effect on ENSO amplitude, individual ensemble runs showed varying results. Earlier studies present conflicting reports on this matter. Dommenget et al. (2006) showed that Atlantic variability damps ENSO, Frauen and Dommenget (2012) showed no net influence, and Sasaki at al. (2014) showed that ENSO amplitude is reduced when the equatorial Atlantic is decoupled. We see both ENSO damping and enhancement in different 100-year runs when the Atlantic alone is decoupled. It is likely that the interaction may be related to multi-decadal variations in the Atlantic-Pacific connection (Rodríguez-Fonseca et al. 2009; McGregor et al. 2014; Sasaki et al. 2014; Kucharski et al. 2016). The inconsistency in the Atlantic-Pacific Niño/Niña relationship is also exhibited in the large CMIP5 multi-model spread clustering around zero (Fig. 9c,d). This spread highlights the need for multiple ensemble experiments and, in light of model biases, the necessity to repeat experiments with several different models.

Since coupled models tend to suffer from the pervasive Indo-Pacific cold tongue bias and strong climatological biases in the tropical Atlantic (Ritcher et al. 2014), alternative decoupling techniques may be necessary to further explore these connections. For example, one could nudge SST over a decoupled region toward observed SST, as conducted by Terray et al. (2015). In this way, biases would be eliminated, however the associated analyses would be confounded by additional mean-state changes, which introduce further complexity. Adding to the complexity is that climatological biases also translate to biases in the modes of variability. One clear example is the shallow thermocline bias in the eastern Indian Ocean that tends to make simulated IOD events notably stronger than observed. However, an error-compensating effect may also occur. Namely, as air-sea coupling tends to be more active in the strong convective region of the Indo-Pacific warm pool, the cold bias may underestimate the remote effect of the IOD, but this should be to a certain extent compensated by the overly large IOD amplitude (Santoso et al. 2012). Thus, while the result may not be greatly affected by this particular bias due to such an error-compensating tendency, a multi-model approach with less biased models seems to be the way forward. The Mk3L model used here exhibits reasonable skill in simulating the tropical modes of climate variability, especially relative to the CMIP5 models that are of higher resolution (Fig. 2). The ensemble spread of index correlations also lies within the CMIP5 multi-model spread in each case (Fig. 9). Therefore, combined with its coarser resolution, the model we employed is particularly useful for studying these types of problems over centennial and millennial timescales. However, it should be further noted that in our case flux adjustments have been employed in order to maintain a more realistic climatology.

Our study highlights the coupling across tropical modes of variability, linked by the atmospheric Walker Circulation. This carries an important implication in that understanding, predicting, and projecting each mode of variability would require a careful consideration of other remote modes of variability. Such coupling also implies that diagnosing interactive feedback, relying on statistical inferences alone, is challenging. We illustrated this challenge by utilising an analysis of CMIP5 models (Fig. 9). For instance, there is a tendency for stronger ENSO and IOBM amplitude to be associated with higher ENSO-IOBM coherence across the models (Fig. 9g,h). At best, this relationship would suggest the IOBM is a mere slave to ENSO. However, with the aid of decoupling experiments in this study and others, the IOBM has been shown to have a damping effect on ENSO. This study provides a basis for understanding the interactions between the dominant modes of variability in the tropics. We note that weaker modes in the tropical domain, for example, the Madden-Julian Oscillation or the Atlantic Meridional Mode, may also influence the interactions that impact on strengths, periods, or predictability of these modes. Furthermore, modes outside of the tropical domain, such as the Southern Annular Mode or the North Atlantic Oscillation, may also have an influence. How these other modes impact on the tropical interactions is a complex topic of investigation that should be explored in future studies.

References

Alexander, M. A., I. Bladé, M. Newman, J. R. Lanzante, N.-C. Lau, and J. D. Scot, 2002: The atmospheric bridge: The influence of ENSO teleconnections on air-sea interaction over the global oceans. J. Clim., 15, 2205–2231.

Annamalai, H., R. Murtugudde, J. Potemra, S. P. Xie, P. Liu, and B. Wang, 2003: Coupled dynamics over the Indian Ocean: Spring initiation of the zonal mode. Deep Sea Res. II, 50, 2305–2330.

Annamalai, H., S. P. Xie, J. P. McCreary, and R. Murtugudde, 2005: Impact of Indian Ocean sea surface temperature on developing El Niño. J. Clim., 18, 302–319.

Baquero-Bernal, A., M. Latif, and S. Legutke, 2002: On dipolelike variability of sea surface temperature in the tropical Indian Ocean. J. Clim., 15, 1358–1368.

Barsugli, J. J. and D. S. Battisti, 1998: The basic effects of atmosphere-ocean thermal coupling on midlatitude variability. J. Atmos. Sci., 55, 477–493.

Behera, S. K., J.-J. Luo, S. Masson, P. Delecluse, S. Gualdi, A. Navarra, and T. Yamagata, 2005: Paramount impact of the Indian Ocean Dipole on the East African short rains: A CGCM study. J. Clim., 18, 4514–4531.

Behera, S. K., J.-J. Luo, S. Masson, S. A. Rao, H. Sakuma, and T. Yamagata, 2006: A CGCM study on the interaction between IOD and ENSO. J. Clim., 19, 1688–1705.

Cai, W. and T. Cowan, 2013: Why is the amplitude of the Indian Ocean Dipole overly large in CMIP3 and CMIP5 climate models? Geophys. Res. Lett., 40, 1200–1205.

Chang, P., Y. Fang, R. Saravanan, L. Ji, and H. Seidel, 2006: The cause of the fragile relationship between the Pacific El Niño and the Atlantic Niño. Nature, 443, 324–328.

Dayan, H., T. Izumo, J. Vialard, M. Lengaigne, and S. Masson 2015: Do regions outside the tropical Pacific influence ENSO through atmospheric teleconnections? Clim. Dyn. 45, 583–601.

Ding, H., N. S. Keenlyside, and M. Latif, 2012: Impact of the equatorial Atlantic on the El Niño Southern Oscillation. Clim. Dyn., 38, 1965–1972.

Dommenget, D., V. Semenov, and M. Latif, 2006: Impacts of the tropical Indian and Atlantic Oceans on ENSO. Geophys. Res. Lett., 33, L11701.

Du, Y., S.-P. Xie, G. Huang, and K. Hu, 2009: Role of air-sea interaction in the long persistence of El Niño-induced North Indian Ocean warming. J. Clim., 22, 2023–2038.

England, M. H., M. Tomczak, and J. S. Godfrey, 1992: Water-mass formation and Sverdrup dynamics: A comparison between climatology and a coupled ocean–atmosphere model. J. Mar. Syst., 3, 279–306.

England, M. H. and F. Huang, 2005: On the interannual variability of the Indonesian throughflow and its linkage with ENSO. J. Clim., 18, 1435–1444.

Fischer, A., P. Terray, E. Guilyardi, S. Gualdi, and P. Delecluse, 2005: Two independent triggers for the Indian Ocean dipole/zonal mode in a coupled GCM. J. Clim., 18, 3428–3449.

Frauen, C. and D. Dommenget, 2012: Influences of the tropical Indian and Atlantic Oceans on the predictability of ENSO. Geophys. Res. Lett., 39, L02706.

Gordon, A. L., 2005: Oceanography of the Indonesian seas and their throughflow. Oceanography, 18, 14–27.

Guilyardi, E., A. Wittenberg, A. Fedorov, M. Collins, C. Wang, A. Capotondi, G. J. van Oldenborgh, and T. Stockdale, 2009: Understanding El Niño in ocean-atmosphere general circulation models: progress and challenges. Bull. Amer. Meteor. Soc., 90, 325–340.

Izumo, T., J. Vialard, M. Lengaigne, C. de Boyer Montegut, S. K. Behera, J.-J. Luo, S. Cravatte, S. Masson, and T. Yamagata, 2010: Influence of the Indian Ocean Dipole on following years El Niño. Nat. Geosci., 3, 168–172.

Izumo, T., M. Lengaigne, J. Vialard, J.-J. Luo, T. Yamagata, and G. Madec, 2014: Influence of Indian Ocean Dipole and Pacific recharge on following years El Niño: interdecadal robustness. Clim. Dyn., 42, 291–310.

Jansen, M. F., D. Dommenget, and N. Keenlyside, 2009: Tropical atmosphere-ocean interactions in a conceptual framework. J. Clim., 22, 550–567.

Kajtar, J. B., A. Santoso, M. H. England, and W. Cai, 2015: Indo-Pacific climate interactions in the absence of an Indonesian Throughflow. J. Clim., 28, 5017–5029.

Keenlyside, N. S., H. Ding, and M. Latif, 2013: Potential of equatorial Atlantic variability to enhance El Niño prediction. Geophys. Res. Lett., 40, 2278–2283.

Keenlyside, N. S. and M. Latif, 2007: Understanding equatorial Atlantic interannual variability. J. Clim., 20, 131–142.

Klein, S. A., B. J. Soden, and N. C. Lau, 1999: Remote sea surface temperature variations during ENSO: Evidence for a tropical atmospheric bridge. J. Clim., 12, 917–932.

Kucharski, F., A. Bracco, J. H. Yoo, and F. Molteni, 2008: Atlantic forced component of the Indian monsoon interannual variability. Geophys. Res. Lett., 35, L04706.

Kucharski, F., F. S. Syed, A. Burhan, I. Farah, and A. Gohar, 2015: Tropical Atlantic influence on Pacific variability and mean state in the twentieth century in observations and CMIP5. Clim. Dyn., 44, 881–896.

Kucharski, F., A. Parvin, B. Rodríguez-Fonseca, R. Farneti, M. Martín-Rey, I. Polo, E. Mohino, T. Losada, and C. R. Mechoso, 2016: The teleconnection of the tropical Atlantic to Indo-Pacific sea surface temperatures on inter-annual to centennial time scales: a review of recent findings. Atmosphere, 7(2), 29.

Kug, J.-S. and I.-S. Kang, 2006a: Interactive feedback between ENSO and the Indian Ocean. J. Climate, 19, 1784–1801.

Kug, J.-S., T. Li, S.-I. An, I.-S. Kang, J.-J. Luo, S. Masson, and T. Yamagata, 2006b: Role of the ENSO-Indian Ocean coupling on ENSO variability in a coupled GCM. Geophys. Res. Lett., 33, L09710.

Latif, M. and A. Grötzner, 2000: The equatorial Atlantic oscillation and its response to ENSO. Clim. Dyn. 16, 213–218.

Latif, M., 2001: Tropical Pacific/Atlantic Ocean interactions at multi-decadal time scales. Geophys. Res. Lett., 28 (3), 539–542.

Lau, N.-C. and M. J. Nath, 1996: The role of the “atmospheric bridge” in linking tropical Pacific ENSO events to extratropical SST anomalies. J. Clim. 9, 2036–2057.

Lau, N.-C. and M. J. Nath, 2003: Atmosphere-ocean variations in the Indo-Pacific sector during ENSO episodes. J. Clim., 16, 3–20.

Losada, T., B. Rodríguez-Fonseca, I. Polo, S. Janicot, S. Gervois, F. Chauvin, and P. Ruti, 2010: Tropical response to the Atlantic Equatorial mode: AGCM multimodel approach. Clim. Dyn., 35, 45–52.

Lübbecke, J. F. and M. J. McPhaden, 2012: On the inconsistent relationship between Pacific and Atlantic Niños. J. Clim., 25, 4294–4303.

Luo, J.-J., R. Zhang, S. K. Behera, Y. Masumoto, F.-F. Jin, R. Lukas, and T. Yamagata, 2010: Interaction between El Niño and extreme Indian Ocean dipole. J. Climate, 23, 726742.

Martín-Rey, M., B. Rodríguez-Fonseca, I. Polo, and F. Kucharski, 2014: On the Atlantic-Pacific Niños connection: a multidecadal modulated mode. Clim. Dyn., 43, 3163–3178.

McGregor, S., A. Timmermann, M. F. Stuecker, M. H. England, M. Merrifield, F.-F. Jin, and Y. Chikamoto, 2014: Recent Walker circulation strengthening and Pacific cooling amplified by Atlantic warming. Nature Clim. Change, 4, 888–892.

Meyers, G., 1996: Variation of Indonesian throughflow and ENSO. J. Geophys. Res., 101, 12,255–12,264.

Phipps, S. J., 2010: The CSIRO Mk3L climate system model v1.2. Tech. rep., Antarctic Climate and Ecosystems Cooperative Research Centre, 121 pp., Hobart, Tas, Australia.

Phipps, S. J., H. V. McGregor, J. Gergis, A. J. E. Gallant, R. Neukom, S. Stevenson, D. Ackerley, J. R. Brown, M. J. Fischer, and T. D. van Ommen, 2013: Paleoclimate data-model comparison and the role of climate forcings over the past 1500 years. J. Clim., 26, 6915–6936.

Polo, I., M. Martín-Rey, B. Rodríguez-Fonseca, F. Kucharski, and C. R. Mechoso, 2014: Processes in the Pacific La Niña onset triggered by the Atlantic Niño. Clim. Dyn., 44, 115–131.

Potemra, J. T., 1999: Seasonal variations of upper-ocean transport from the Pacific to the Indian Ocean via Indonesian Straits. J. Phys. Oceanogr., 29, 2930–2944.

Richter, I., S. P. Xie, S. K. Behera, T. Doi, and Y. Masumoto, 2014: Equatorial Atlantic variability and its relation to mean state biases in CMIP5. Clim. Dyn., 42, 171–188.

Rodrigues, R. R., R. J. Haarsma, E. J. D. Campos, and T. Ambrizzi, 2011: The impacts of inter-El Niño variability on the tropical Atlantic and northeast Brazil climate. J. Clim., 24, 3402–3422.

Rodríguez-Fonseca, B., I. Polo, J. García-Serrano, T. Losada, E. Mohino, C. R. Mechoso, and F. Kucharski, 2009: Are Atlantic Niños enhancing Pacific ENSO events in recent decades? Geophys. Res. Lett., 36, L20705.

Santoso, A., A. Sen Gupta, and M. H. England, 2010: Genesis of Indian Ocean mixed layer temperature anomalies: A heat budget analysis. J. Clim., 23, 5375-5403.

Santoso, A., W. Cai, M. H. England, and S. J. Phipps, 2011: The role of the Indonesian Throughflow on ENSO dynamics in a coupled climate model. J. Clim., 24, 585–601.

Santoso, A., M. H. England, and W. Cai, 2012: Impact of Indo-Pacific feedback interactions on ENSO dynamics diagnosed using ensemble climate simulations. J. Clim., 25, 7743–7763.

Saravanan, R. and P. Chang, 2000: Interaction between tropical Atlantic variability and El Niño-Southern Oscillation. J. Clim., 13, 2177–2195.

Sasaki, W., T. Doi, K. J. Richards, and Y. Masumoto, 2014: Impact of the equatorial Atlantic sea surface temperature on the tropical Pacific in a CGCM. Clim. Dyn., 43, 2539–2552.

Sprintall, J., and A. Révelard, 2014: The Indonesian Throughflow response to Indo-Pacific climate variability. J. Geophys. Res. Oceans, 119, 1161–1175.

van Sebille, E., J. Sprintall, F. U. Schwarzkopf, A. S. Gupta, A. Santoso, M. H. England, A. Biastoch, and C. W. Böning, 2014: Pacific-to-Indian Ocean connectivity: Tasman leakage, Indonesian Throughflow, and the role of ENSO. J. Geophys. Res. Oceans, 119, 1365–1382.

Taschetto, A. S., R. R. Rodrigues, G. A., Meehl, S., McGregor, and M. H. England, 2016: How sensitive are the Pacific–tropical North Atlantic teleconnections to the position and intensity of El Niño-related warming? Clim. Dyn., 46, 1841–1860.

Terray, P., S. Masson, C. Prodhomme, M. K. Roxy, and K. P. Sooraj, 2016: Impacts of Indian and Atlantic oceans on ENSO in a comprehensive modeling framework. Clim. Dyn., 46, 2507–2533.

Vranes, K., A. L. Gordon, and A. Ffield, 2002: The heat transport of the Indonesian throughflow and implications for the Indian Ocean heat budget. Deep-Sea Res. II, 49, 1391–1410.

Wang, B., R. Wu, and R. Lukas, 1999a: Role of the western North Pacific wind variation in thermocline adjustment and ENSO phase transition. J. Meteor. Soc. Japan, 77, 1–16.

Wang, C., R. H. Weisberg, and J. I. Virmani 1999b: Western Pacific interannual variability associated with the El Niño-Southern Oscillation, J. Geophys. Res., 104(C3), 5131–5149.

Watanabe, M., and F.-F. Jin, 2002: Role of Indian Ocean warming in the development of Philippine Sea anticyclone during ENSO, Geophys. Res. Lett., 29(10), 1478.

Wijffels, S. E., G. Meyers, and J. S. Godfrey, 2008: A 20-yr average of the Indonesian throughflow: Regional currents and the interbasin exchange. J. Phys. Oceanogr., 38, 1965–1978.

Wu, R. and B. P. Kirtman, 2004: Understanding the impacts of the Indian Ocean on ENSO variability in a coupled GCM. J. Clim., 17, 4019–4031.

Yu, J.-Y., C. R. Mechoso, J. C. McWilliams, and A. Arakawa, 2002: Impacts of the Indian Ocean on the ENSO cycle. Geophys. Res. Lett., 29, 1204.

Yuan, D., H. Zhou, and X. Zhao, 2013: Interannual climate variability over the tropical Pacific ocean induced by the Indian ocean dipole through the Indonesian throughflow. J. Clim., 26, 2845–

2861.

Zebiak, S. E., 1993: Air-sea interaction in the equatorial Atlantic region. J. Clim., 6, 1567–1586.

Tropical Climate Variability: Interactions across the Pacific, Indian, and Atlantic Oceans

Jules B. Kajtar*[1,2], Agus Santoso[1,2], Matthew H. England[1,2], and Wenju Cai[3]

[1] ARC Centre of Excellence for Climate System Science, University of New South Wales, NSW, Australia

[2] Climate Change Research Centre, University of New South Wales, NSW, Australia

[3] CSIRO Marine and Atmospheric Research, Aspendale, Victoria, Australia

* Corresponding author: Jules B. Kajtar, j.kajtar@unsw.edu.au

Tables and Figures

TABLE 1. Summary of the tropical modes of variability considered in this study.

Mode	*Ocean*	*Characteristic SST Index*	*SST Averaging Area*	*Peak Season*
El Niño-Southern Oscillation (ENSO)	Pacific	Niño-3.4	5ºS-5ºN, 170º-120ºW	September to December (SOND)
Atlantic Equatorial Mode (AEM)	Atlantic	Atl-3	5ºS-5ºN, 20ºW-0º	June to August (JJA)
Indian Ocean Dipole (IOD)	Indian	Dipole Mode Index (DMI)	west (10ºS-10ºN, 50º-70ºE) minus east (10ºS-0º, 90º-110ºE)	August to November (ASON)
Indian Ocean Basinwide Mode (IOBM)	Indian	Basinwide Index (BWI)	20ºS-20ºN, 40º-100ºE	January to April (JFMA)

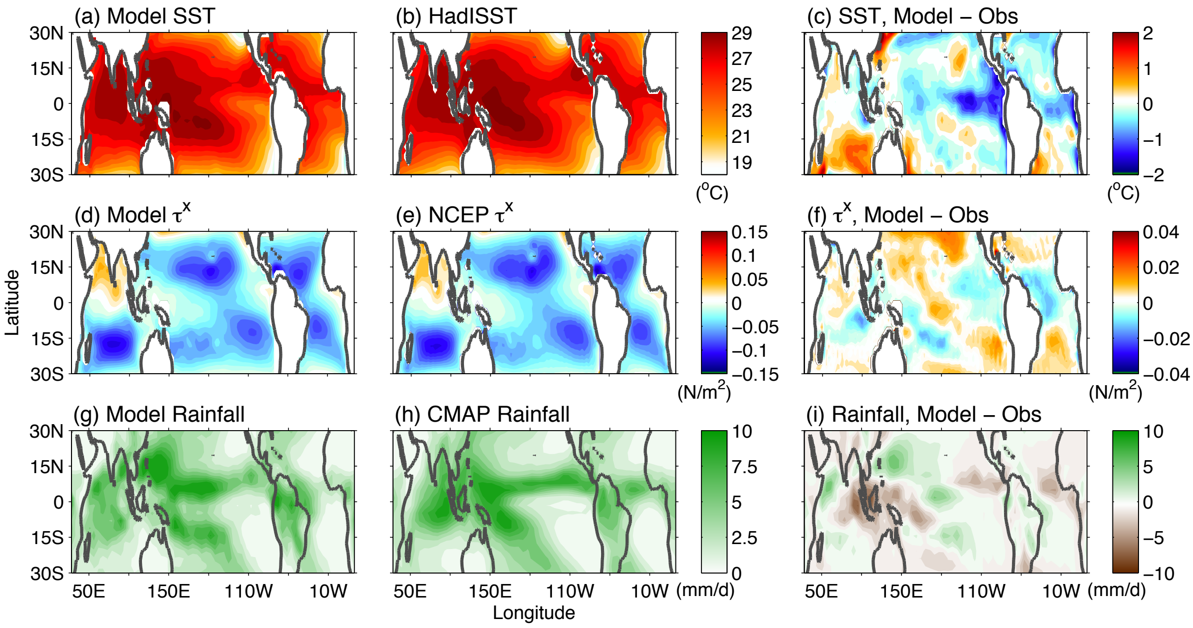

Fig. 1 Comparison of the Mk3L model SST, winds, and rainfall with observed data. (a) Model SST, (b) HadISST (averaged over 1900-2010), and (c) difference between model and observed SST. (d) Model zonal wind stress (τ^x), (e) NCEP-NCAR reanalysis τ^x (averaged over 1948-2010), and (f) difference between model and observed τ^x. (g) Model rainfall, (h) Climate Prediction Center Merged Analysis of Precipitation (CMAP) reanalysis rainfall (averaged over 1979-2010), and (i) difference between model and observed rainfall. The model climatology is averaged over the entire 300 years of the original CTRL run.

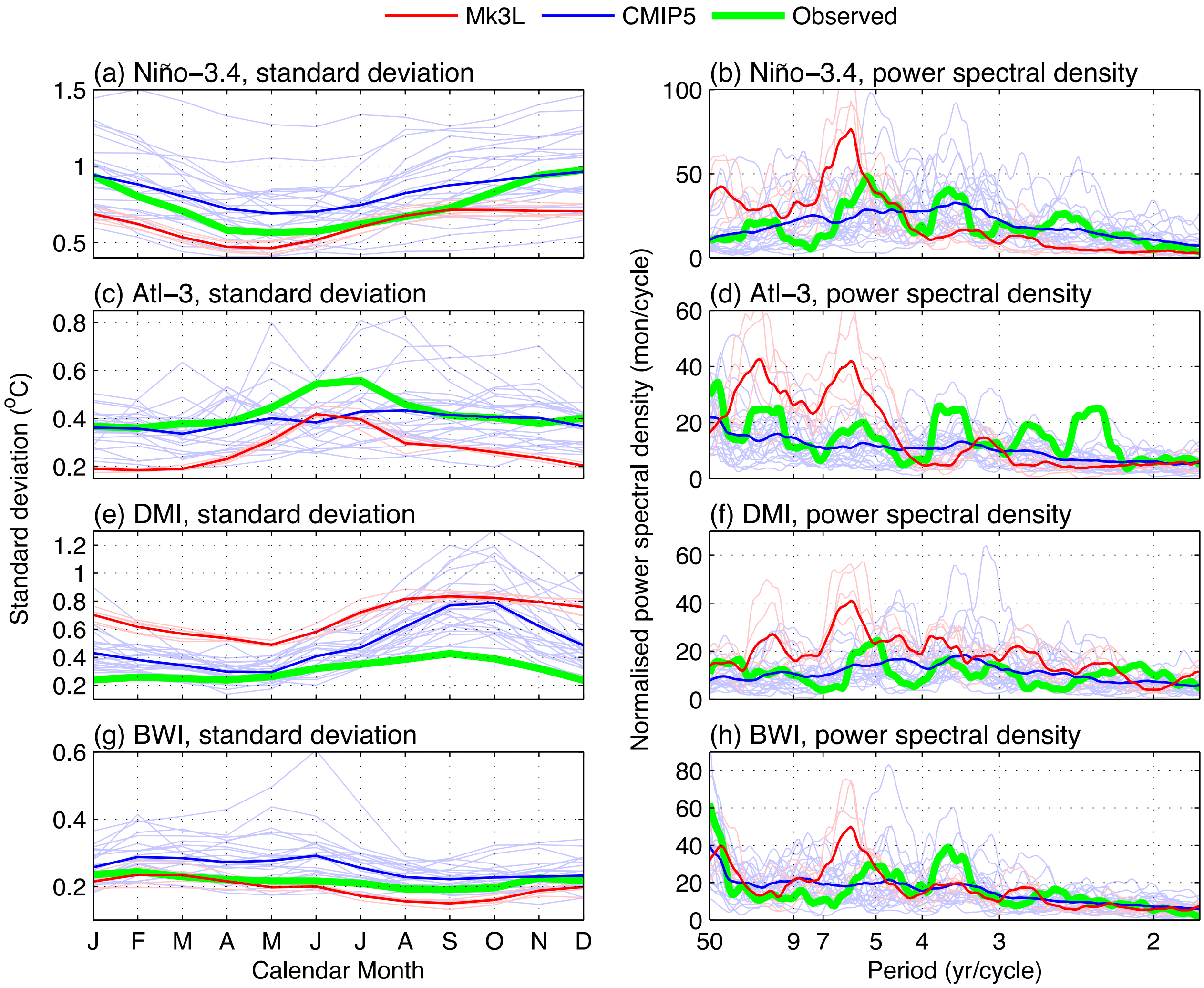

Fig. 2 Monthly standard deviation and power spectral densities (PSDs) of the SST indices characterizing the dominant modes of tropical climate variability. (a,b) Niño-3.4, which characterizes the El Niño-Southern Oscillation. (c,d) Atl-3, for the Atlantic Equatorial Mode. (e,f) DMI, for the Indian Ocean Dipole. (g,h) BWI, for the Indian Ocean Basinwide Mode. The faint red curves denote the five ensemble members of the CTRL experiment in Mk3L, with the bold red curve denoting the ensemble mean. The faint blue curves denote individual historical CMIP5 model runs (Section 2.2), with the bold blue curve denoting the CMIP5 mean. The green curve denotes the observed from the HadISST set. For easier comparison, the time-series are normalised to unity variance before computing the PSDs. Note that the individual CMIP5 models are not distinguished, since they are presented purely to indicate the multi-model spread.

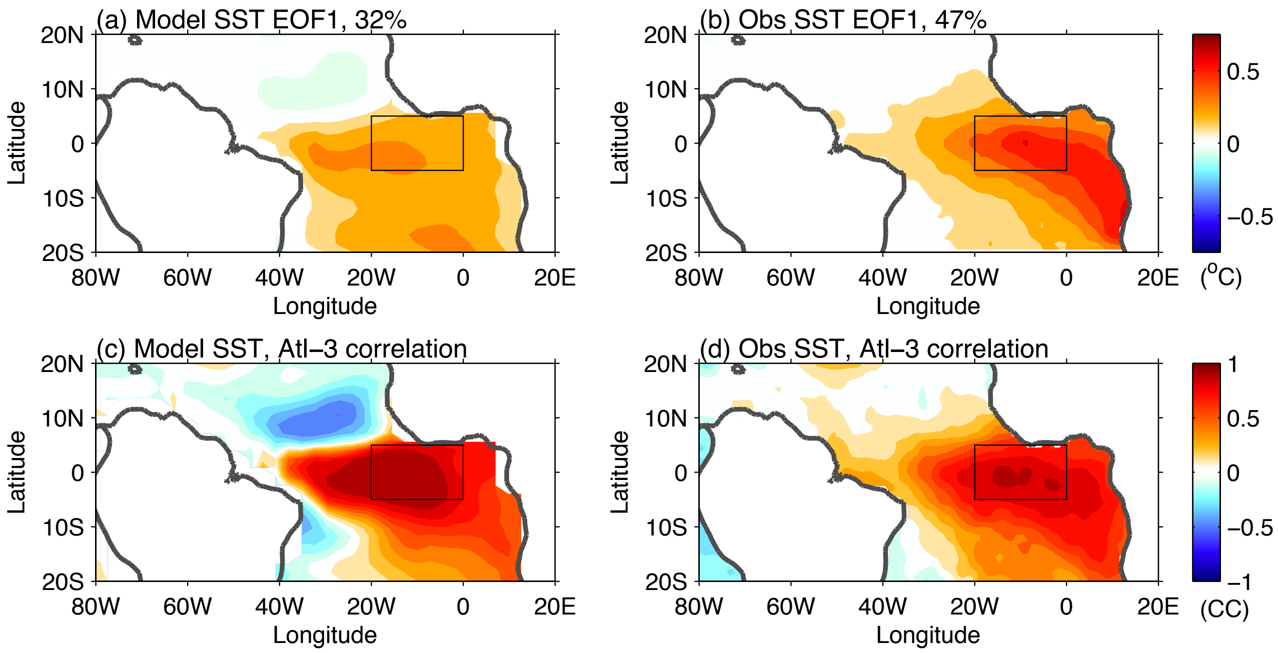

Fig. 3 First empirical orthogonal function (EOF) of June to August Atlantic SST presented as a regression map, showing the pattern for the Atlantic equatorial mode for (a) the model and (b) HadISST. The variances explained by the first EOFs are given in the panel titles. (c,d) Correlation coefficients of Atl-3 index with SST field, using June to August mean in each case. The EOF analysis is for the entire 300 years of the original model CTRL run, and over 1900 to 2010 for HadISST.

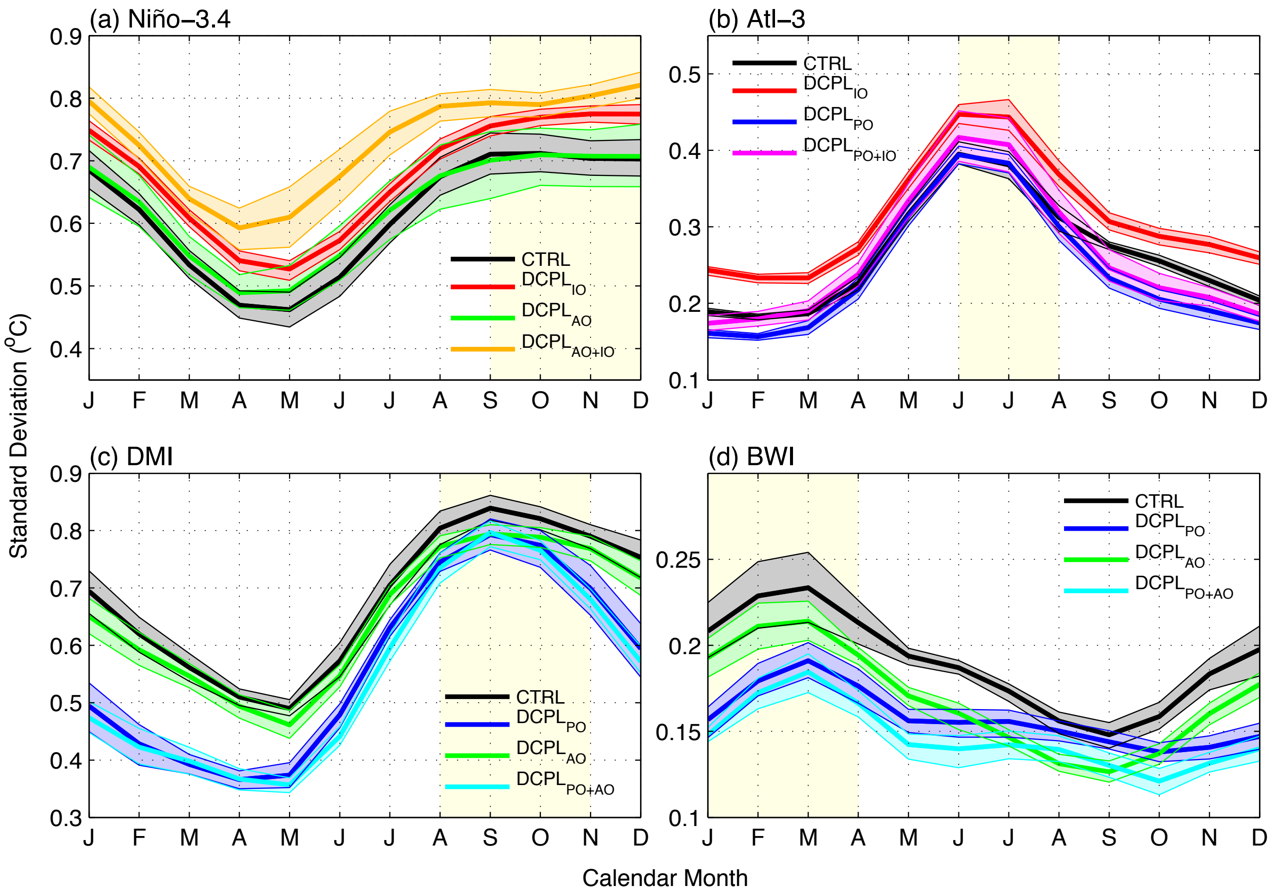

Fig. 4 Monthly standard deviation of SST indices representing the dominant modes of tropical climate variability: (a) Niño-3.4 for the Pacific Ocean, (b) Atl-3 for the Atlantic Ocean, (c) Dipole Mode Index, and (d) Basinwide Index for the Indian Ocean. The results for the CTRL and the various partial coupling experiments are shown. A low-pass filter with a 4-month cut-off was applied to smooth each time-series before computing the monthly standard deviations. The color-shaded areas indicate the 95% confidence intervals, which were estimated based on 1000 bootstrapped means from the five 100-year ensemble members. The borders of the shaded regions are outlined for clarity. The months shaded in yellow indicate the peak season of variability of each mode, upon which further analysis in the text is focussed.

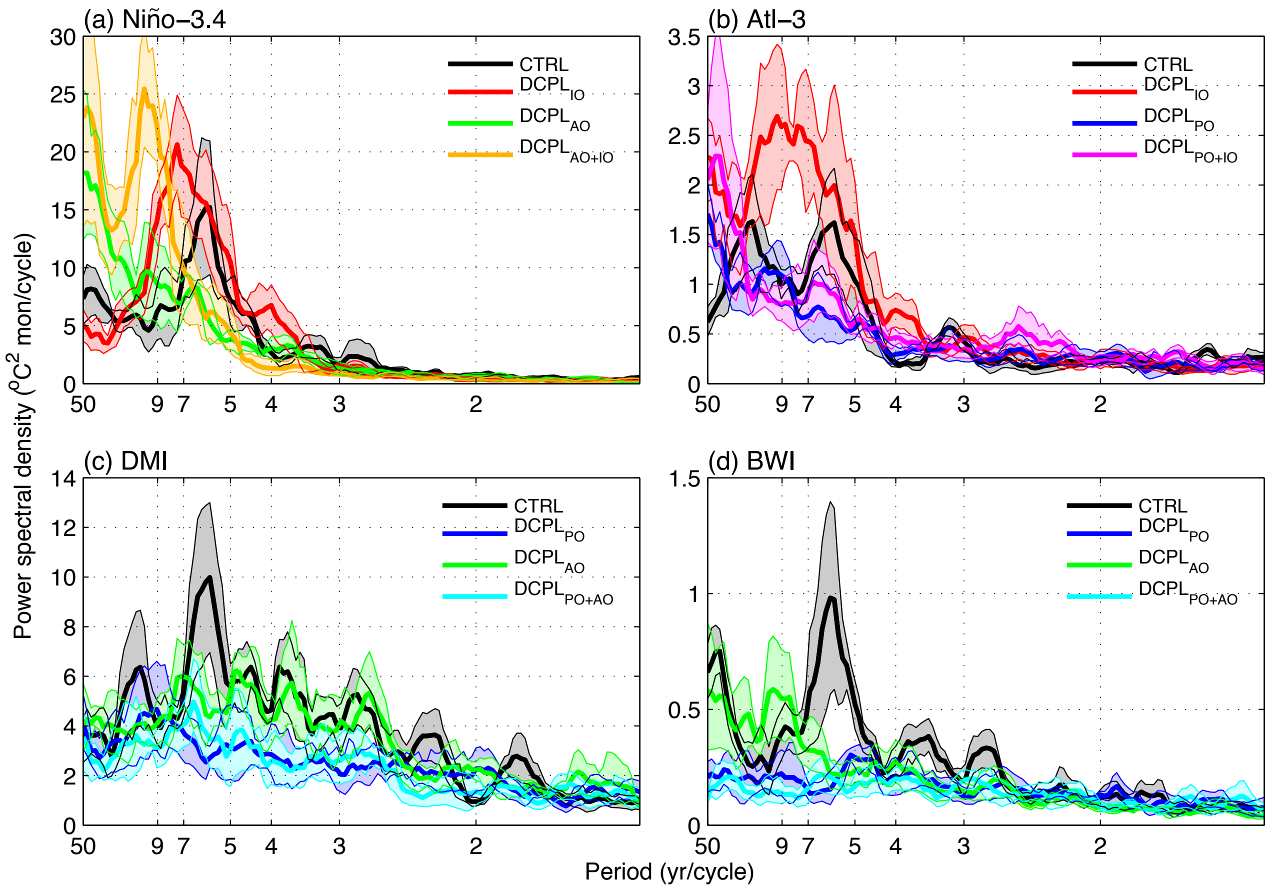

Fig. 5 Power spectral densities of the same SST indices shown in Fig. 4.

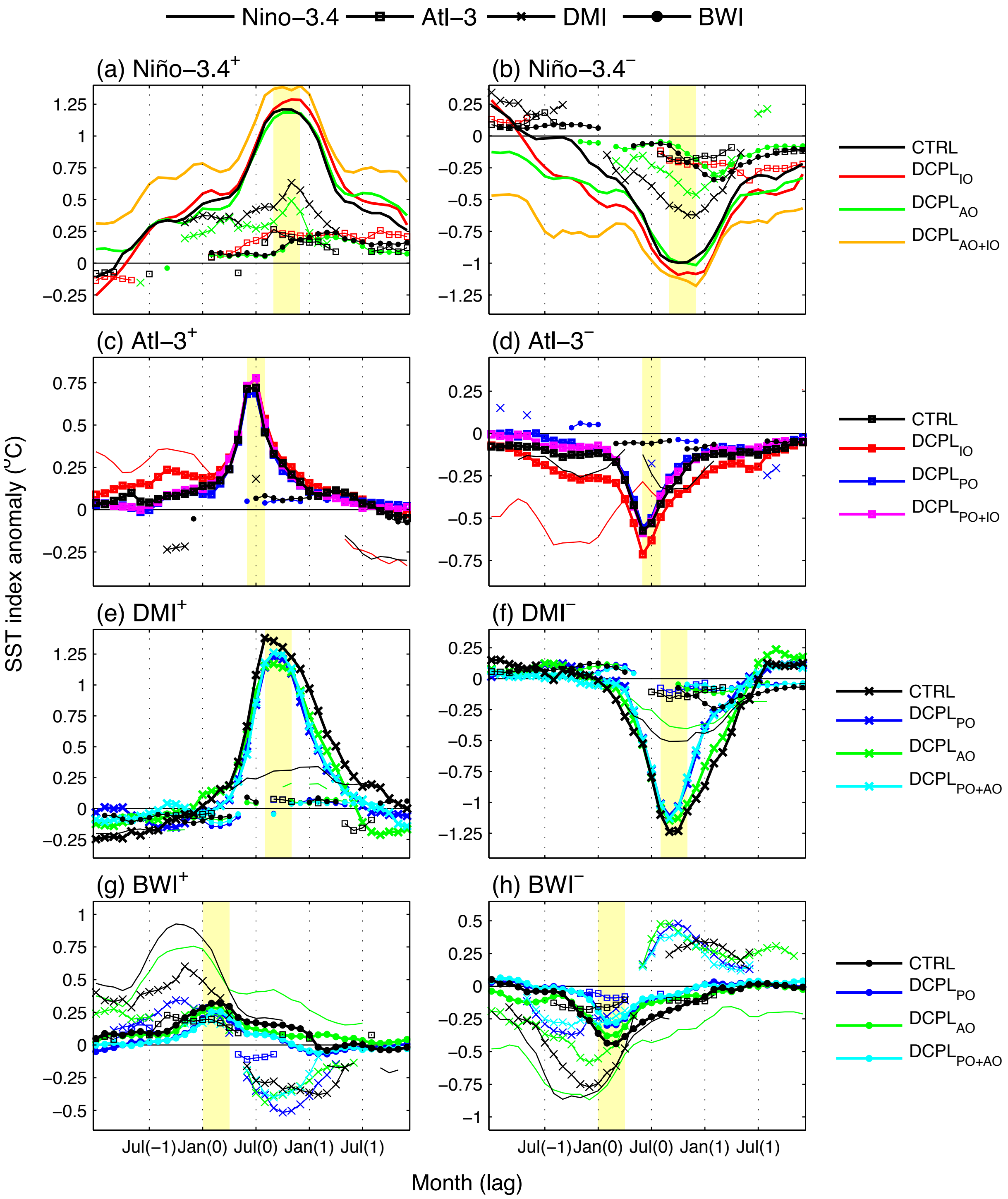

Fig. 6 Composite evolution of tropical climate mode events for each SST index over a 36-month period. Events are composited as described in Section 4. The different lines styles denote the different indices throughout the figure: solid lines for Niño-3.4, lines with squares for Atl-3, lines with crosses for DMI, and lines with circles for BWI. The colours denote the different experiments. (a) Composite evolution of the Niño-3.4 index for El Niño events (thick, solid lines), in CTRL (black) and each of the partially coupled experiments ($DCPL_{IO}$: red, $DCPL_{AO}$: green, $DCPL_{AO+IO}$: orange). Alongside is the co-evolution of each of

the other indices (thin lines, and again, line styles and colors indicate the different indices and experiments). (b) Composite evolution of the Niño-3.4 index for La Niña events. (c,d) Composite evolution of Atl-3 for warm and cool AEM events, respectively. (e,f) Composite evolution of DMI for positive and negative IOD events, respectively. (g,h) Composite evolution of BWI for warm and cool IOBM events, respectively. Apart from the evolutions of main index in each panel (thick lines), which are plotted for the entire 36-month span, only those periods for which the other indices are significantly different from zero at the 95% confidence level under a *t*-test are shown (thin lines). Jul(0) denotes July in the year of the event, and -1 or 1 denotes the year prior or ahead. Year 0 is relative to the peak of each mode. The months shaded in yellow indicate the peak seasons of variability for the main index in each panel (Table 1).

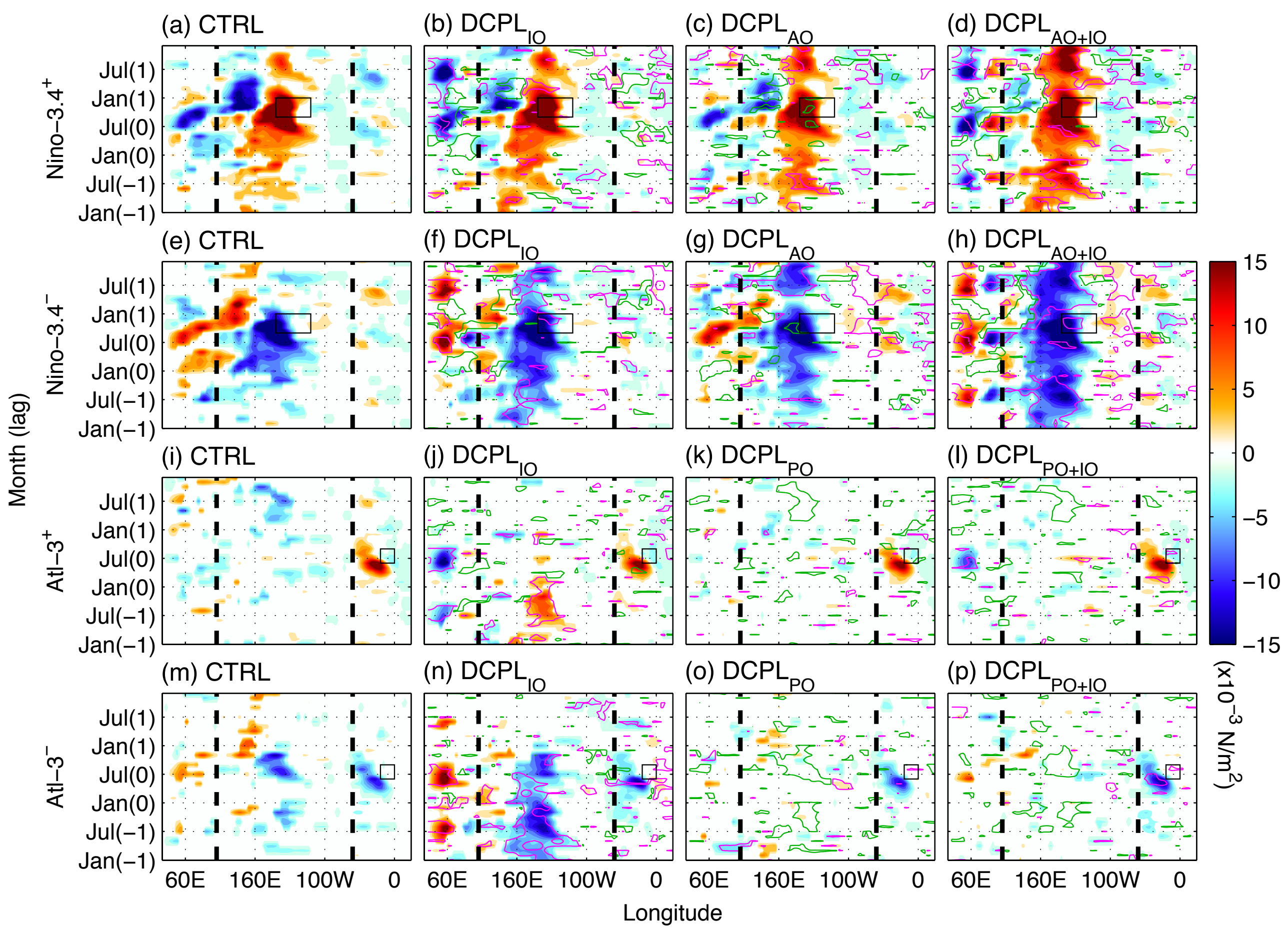

Fig. 7 Composites of equatorial zonal surface wind stress anomalies over a 36-month period associated with ENSO and AEM events. (a) El Niño composites in CTRL. (b-d) El Niño composites in each of the relevant decoupling experiments. (e-h) La Niña composites. (i-l) Atlantic Niño composites. (m-p) Atlantic Niña composites. Events are composited as described in Section 4. Only the wind stresses that are significantly different from zero at the 95% confidence level under a *t*-test are shaded. The zonal wind stress is averaged over 5ºS-5ºN. The vertical dashed lines indicate the approximate boundaries between the ocean basins. The box in each panel indicates the spatial and temporal extent of relevant composited index. On the DCPL panels, the pink contours indicate where $|DCPL| - |CTRL|$ is positive and significant above the 90% level. The green contours indicate where $|DCPL| - |CTRL|$ is negative and significant above the 90% level.

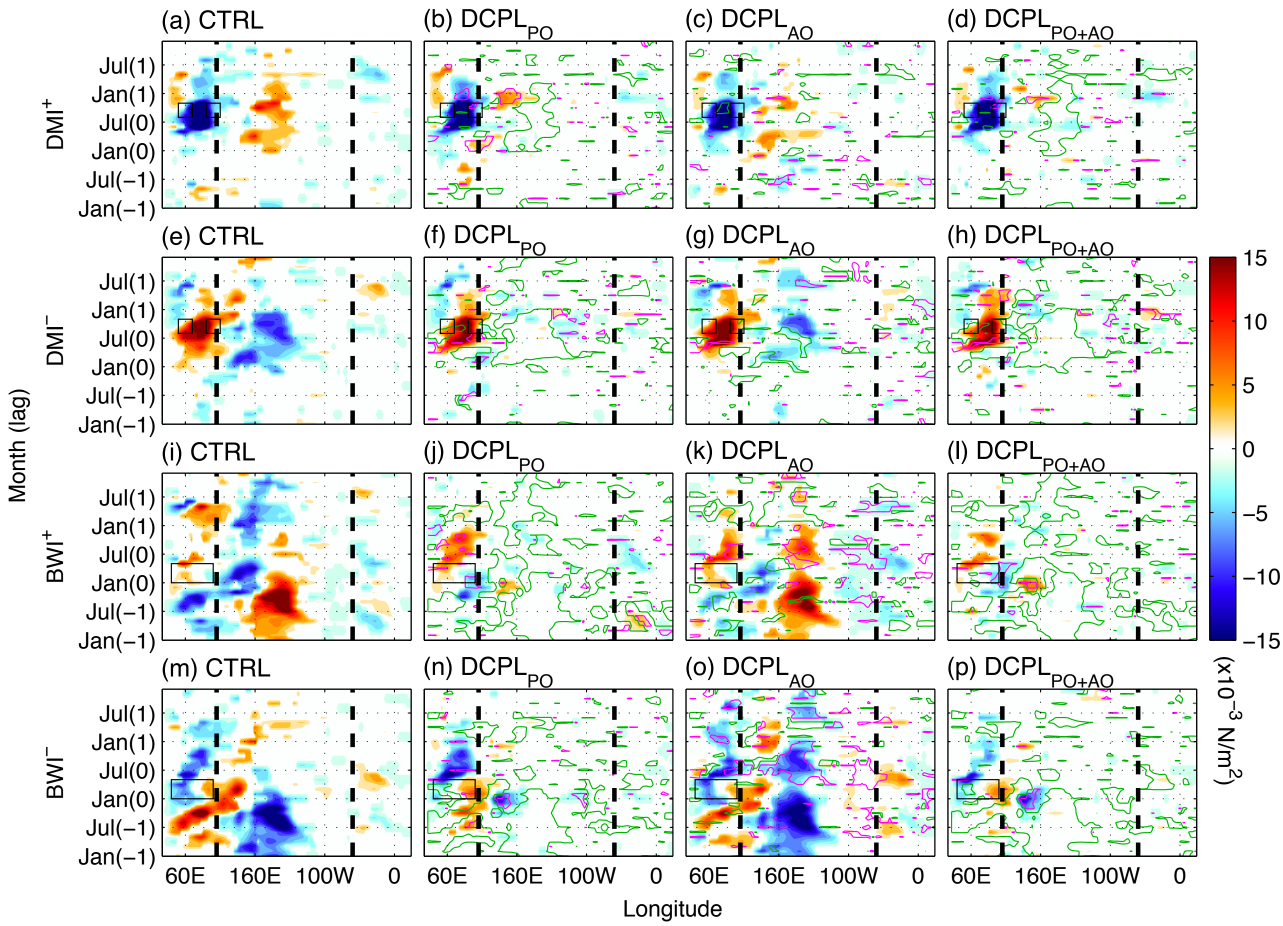

Fig. 8 As in Fig. 7 but for IOD and IOBM events. (a) Positive IOD composites in CTRL. (b-d) Positive IOD composites in each of the relevant decoupling experiments. (e-h) Negative IOD composites. (i-l) Warm IOBM composites. (m-p) Cool IOBM composites.

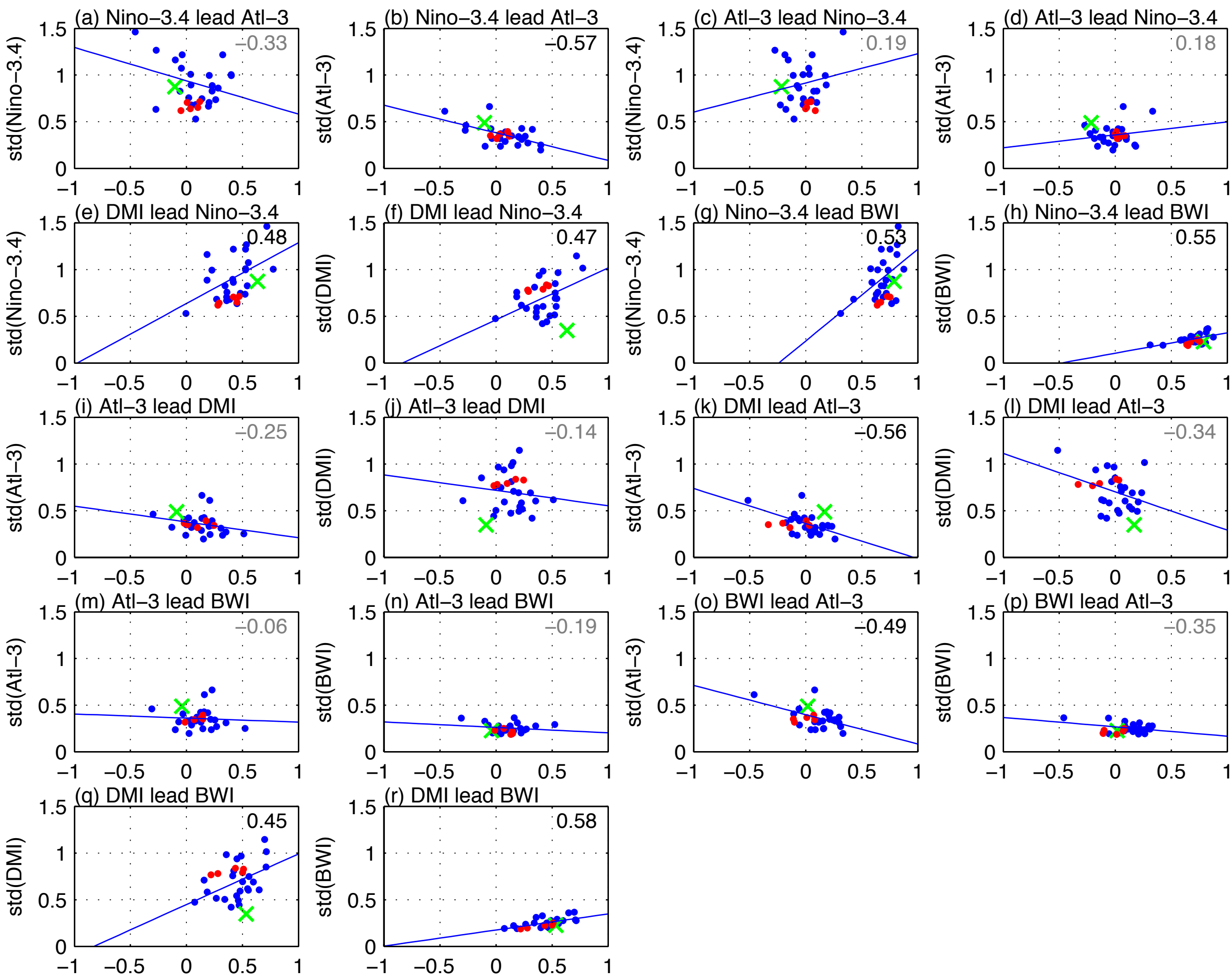

Fig. 9 Correlation coefficients between pairs of indices plotted against the standard deviation of each in the pair. Annual averages are taken for each index over the following months: DJF for Niño-3.4, JJA for Atl-3, SON for DMI, and JFM for BWI. The months here were chosen based on the observed peak season of variability, rather than the peak seasons of the modes in the model. The blue dots denote individual CMIP5 historical runs (over the period 1900-1999) with blue lines of best-fit, the red dots denote the 100-year Mk3L CTRL ensemble members, and the green crosses denote the HadISST observations (1900-1999). The CMIP5 inter-model correlation coefficient is given in each panel, where a black value indicates that the correlation is significant at the 95% level, and grey is not significant.